JACS
JOURNAL OF THE AMERICAN CHEMICAL SOCIETY
Communication
pubs.acs.org/JACS

Low-Voltage Organic Field Effect Transistors with a 2-Tridecyl[1]benzothieno[3,2-*b*][1]benzothiophene Semiconductor Layer

Atefeh Y. Amin,[§] Artoem Khassanov,[§] Knud Reuter,[#] Timo Meyer-Friedrichsen,[#] and Marcus Halik*[,§]

[§]Organic Materials & Devices, Institute of Polymer Materials, Department of Materials Science, University of Erlangen-Nürnberg, Martensstraße 7, 91058 Erlangen, Germany

[#]Heraeus Precious Metals GmbH&Co. KG, Chempark Leverkusen, Building B202, 51368 Leverkusen, Germany

Supporting Information

ABSTRACT: An asymmetric *n*-alkyl substitution pattern was realized in 2-tridecyl[1]benzothieno[3,2-*b*][1]-benzothiophene (C_{13}-BTBT) in order to improve the charge transport properties in organic thin-film transistors. We obtained large hole mobilities up to 17.2 $cm^2/(V{\cdot}s)$ in low-voltage operating devices. The large mobility is related to densely packed layers of the BTBT π-systems at the channel interface dedicated to the substitution motif and confirmed by X-ray reflectivity measurements. The devices exhibit promising stability in continuous operation for several hours in ambient air.

Tailor-made organic materials play an important role when it comes to bringing organic field effect transistors (OFETs) closer to market applications. Chemical modifications address such properties as cost-efficient processability, long-term stability, improved morphology, etc., which are essential secondary properties besides large charge carrier mobilities.[1−4] Prominent examples of such new high-performance semiconductive molecules are benzo- and naphtho-fused thienothiophenes.[5] 2,7-Dialkyl[1]benzothieno[3,2-*b*][1]-benzothiophenes (BTBTs) in particular have shown remarkable charge carrier mobilities of up to 16.4 $cm^2/(V{\cdot}s)$ in single crystals and 2.75 $cm^2/(V{\cdot}s)$ in polycrystalline films.[4,5] So far, only symmetric examples of C_n-BTBT-C_n (*n*-alkyl chains from n = 2 to 14) have been investigated in OFETs, mainly with longer alkyl chains ($n \geq 8$) because longer alkyl chains improve the solubility and enable processing from solution.[6,4] From the electronics point of view, however, long alkyl chains create bulky insulating layers between the semiconducting $\pi-\pi$ stacks along the polycrystalline thin film, which limits the vertical transport (injection and extraction) and dilutes the number of π-systems very close at the channel interface. Despite this, the alkyl chain motif facilitates further improvement of the BTBT system via smart chemical design. The shortening of alkyl side chains, for example, is a promising approach to reach larger charge carrier mobilities in OFETs, as demonstrated in α,ω-alkyl-substituted oligothiophenes (e.g., n = 2),[7] but it also exhibits problems in the homogeneous film formation for BTBTs due to the their high tendency to crystallize. In contrast to oligothiophenes, however, the monofunctionalization of BTBT (C_n-BTBT) does not affect the operational stability of devices in ambient condition because of the high HOMO level of the BTBT π-system (E_{HOMO} = −5.8 eV) and the absence of a reactive α-hydrogen.[2,8]

Here, we report on 2-tridecyl[1]benzothieno[3,2-*b*][1]-benzothiophene (C_{13}-BTBT), which is easily accessible as a high-performance organic semiconductor by common chemistry processes (Scheme 1).[9,10] Polycrystalline films of C_{13}-BTBT were investigated by means of atomic force microscopy (AFM) and X-ray reflectivity (XRR). OFETs with a C_{13}-BTBT semiconductor were fabricated with different ultrathin gate dielectrics to enable low-voltage operation and to exhibit the C_{13}-BTBT performance for different channel interfaces. We obtained large grains (>1 μm) in the polycrystalline films and short distances in the range of 13−14 Å between the π-systems, indicating a dense packaging (Figures 1d and 2). Devices show a large charge carrier mobility of up to 17.2 $cm^2/(V{\cdot}s)$, and their performance depends on the dielectric surface, which influences the molecular order of the first C_{13}-BTBT monolayers at the dielectric surface.

Scheme 1. Synthetic Approach for C_{13}-BTBT

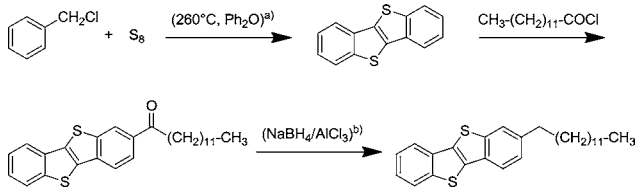

[a]The procedure from ref 9 was modified to gently refluxing diphenyl ether at 260 °C. Process control, workup, and yield (45%) were improved by this method. [b]Instead of hydrazine,[9] sodium boranate/aluminum chloride[10] was used for reduction.

C_{13}-BTBT was synthesized similarly to the literature method[9] with two modifications as described in Scheme 1. The final product was purified by recrystallization from ethanol.

Top-contact bottom-gate transistors were fabricated following the same methods as described recently.[11] The gate electrodes (Al 30 nm) were evaporated on Si/SiO_2 substrates through a stencil mask. In order to create the hybrid dielectric, the substrate was treated with oxygen plasma, yielding a 3.6 nm

Received: August 9, 2012
Published: September 25, 2012

dx.doi.org/10.1021/ja307802q | J. Am. Chem. Soc. 2012, 134, 16548−16550

Table 1. Experimental Characteristics of Field Effect Transistors

dielectric	saturation μ^a at $V_{DS} = -2$ V ($cm^2/(V{\cdot}s)$)	V_{TH} (V)	I_{on}/I_{off}	I_D/I_G	surface energy (mN/m)	average contact angle (°)	measured capacitance per area ($\mu F/cm^2$)
AlO_x	1.17 ± 0.3	−2.2 ± 0.00	3.6×10^3	9.08	52.1	–	1.27×10^{-6}
AlO_x/C_{14}-PA	14.20 ± 2.55	−2.7 ± 0.09	1.60×10^7	1.60×10^3	20.8	110	7.54×10^{-7}
$AlO_x/F_{15}C_{18}$-PA	2.71 ± 0.89	−1.9 ± 0.07	1.90×10^7	1.70×10^4	9.3	120	5.80×10^{-7}
AlO_x/C_{10}-PA	7.10 ± 1.61	−2.8 ± 0.04	3.23×10^7	3.80×10^3	22	109	9.91×10^{-7}

[a]Charge carrier mobility has been extracted from gradual channel approximation in saturation regime. The average values are presented for four different OFETs. Channel length of devices with AlO_x and AlO_x/ClO-PA dielectrics are L = 200 μm; for the rest L = 300 μm; channel width of all measurements is 500 μm.

AlO_x layer on the Al pattern, followed by self-assembly of *n*-decylphosphonic acid (C_{10}-PA), *n*-tetradecylphosphonic acid (C_{14}-PA), or 12,12,13,13,14,14,15,15,16,16,17,17,18,18,18*H*-pentadecafluorooctadecylphosphonic acid ($F_{15}C_{18}$-PA) from 0.2 mM solution in 2-propanol.[11−13] For a better comparison, reference samples with Al/AlO_x (without SAM) were fabricated in parallel. The relevant data (contact angle, surface energy, and capacitance) are summarized in Table 1. The choice of the different SAMs relates to their ability to provide different surface energies for the subsequently deposited C_{13}-BTBT and also to tune the threshold voltage in OFETs.[11,13] C_{13}-BTBT (20 nm) was deposited by thermal evaporation ($p = 10^{-6}$ mbar, rate 0.1 Å/s) on top of the hybrid dielectric through a shadow mask. The substrate was kept at 60 °C during the semiconductor evaporation, which is below the melting point of C_{13}-BTBT (T_m^{DSC} = 106.4 °C, Supporting Information SI-7). The devices were completed by evaporation of gold source and drain electrodes (30 nm) on top. All electrical characterizations were performed in ambient air. Output and transfer characterization at different saturation and linear source−drain voltages were recorded for at least four samples of the same channel width (W = 500 μm) and channel length (L = 300 or 200 μm). The average device values in the saturation regime, extracted from gradual channel approximation, are presented in Table 1. The complete characteristics of representative devices are reported in SI-2. AFM measurements were done in tapping mode for different surfaces. XRR measurements were performed at the beamline ID10B[14] at the ESRF (Grenoble, France) using a monochromatic X-ray beam at λ = 0.93 Å.

Figure 1a,b shows the transfer and output characteristics of a C_{13}-BTBT OFET with AlO_x/C_{14}-PA hybrid gate dielectric. A record value of 17.2 $cm^2/(V{\cdot}s)$ was obtained from this device. The average hole mobility of four representative devices is 14.2 $cm^2/(V{\cdot}s)$, with a large ON/OFF current ratio of 10^7 and an average threshold voltage of V_{TH} = −2.7 V (SI-2). OFETs with a bare AlO_x dielectric layer and C_{10}-PA or $F_{15}C_{18}$-PA SAM dielectrics show slightly reduced average mobilities between 1.17 and 7.1 $cm^2/(V{\cdot}s)$ (Table 1). Devices with AlO_x/SAM hybrid dielectric show an improved ON/OFF current ratio due to the enhanced gate insulation with the SAM. The relatively large negative threshold voltage of V_{TH} = −2.7 V for *n*-alkyl SAMs (C_{10}-PA and C_{14}-PA) and AlO_x dielectrics is shifted to V_{TH} = −1.9 V for $AlO_x/F_{15}C_{18}$-PA according to the negative dipole moment of the fluorinated molecule.[11,13] In order to explain the large mobilities on *n*-alkyl chain SAMs in particular, we have studied the morphology of C_{13}-BTBT in thin films. The AFM image of a 20 nm thick film of C_{13}-BTBT on a C_{14}-PA surface indicates a polycrystalline film with large grains of about 1 μm. However, the early state of the film growth during deposition is of particular importance, as this defines the dielectric−semiconductor interface, and only the first closed

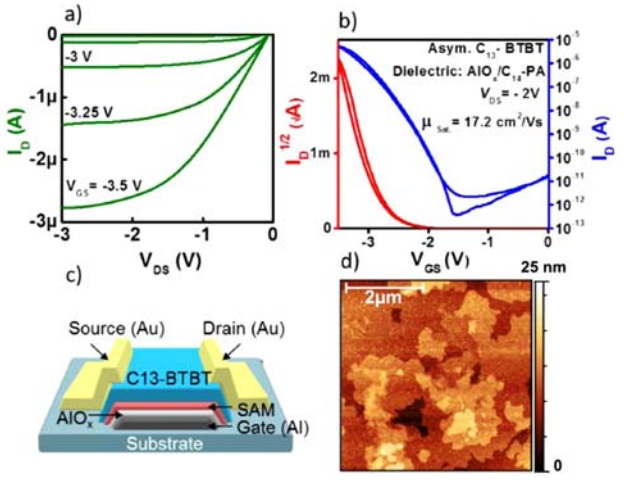

Figure 1. (a) Output characteristics of the best device with AlO_x/C_{14}-PA hybrid dielectric and (b) its corresponding transfer curve. Channel length and width are 200 and 500 μm, respectively. (c) Schematics of top-contact/bottom-gate OFET used in this study. (d) AFM picture of morphology of C_{13}-BTBT thin film of 20 nm.

conductive layers close to the dielectric interface contribute significantly to the charge transport.[15] Figure 2a shows an AFM image of a C_{13}-BTBT submonolayer film deposited on C_{14}-PA. A silicon wafer with 5 nm of atomic layer deposition (ALD) AlO_x, decorated with C_{14}-PA, was used as substrate since it allowed easier access to step height analysis due to the small surface roughness of the ALD oxide ($R_{ms} \approx$ 0.13 nm). Large, smooth islands of C_{13}-BTBT with several hundreds nm diameter were obtained without detectable terracing. The step height of 5.1 nm (Figure 2b) exceeds the nominal length of 2.4 nm for a C_{13}-BTBT molecule, and even the length of a classic double layer with face-to-face stacking of the BTBT π-systems. This suggests a different molecular arrangement (e.g., alternating packaging of the alkyl chains with strong π-stacking of the BTBT units and interlocked alkyl chains; Figure 2b inset). However, a more detailed picture of the molecular packing requires a more surface sensitive method. XRR was applied to the same thin film as used in AFM step height analysis. Figure 2c shows the result of the XRR experiments after fitting to a model scattering length density (SLD) using the Parratt formalism[16] and least-squares analysis. The fitted SLD profile along the *z*-axis shows a periodic signature of increased SLD (π-system) on top of the C_{14}-PA SAM. The periodicity of about 13−14 Å indicates repetition of $\pi-\pi$ stacking (electron rich) every 13−14 Å, with the first peak very close to the interface (<1 nm), simply spaced by the C_{14}-PA SAM. The small periodicity and the peak shapes suggest a densely packed arrangement of BTBT π-systems in the channel region. In order to explain the significant difference in mobility

dx.doi.org/10.1021/ja307802q | J. Am. Chem. Soc. 2012, 134, 16548−16550

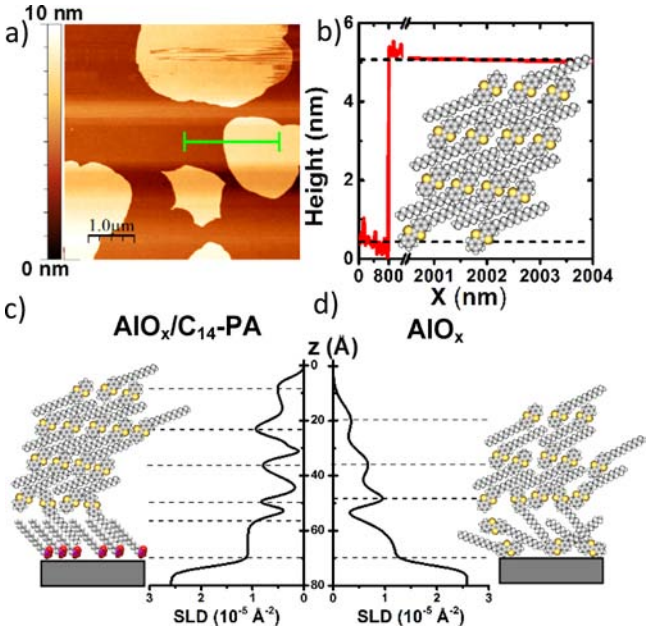

Figure 2. (a) Morphology of submonolayer evaporated C_{13}-BTBT on ALD-AlO_x/C_{14}-PA. (b) Profile of asymmetric C_{13}-BTBT island (green line). (c,d) SLD profiles from XRR experiments of asymmetric C_{13}-BTBT on (c) AlD-AlO_x/C_{14}-PA and (d) AlD-AlO_x in addition to suggested corresponding molecular packaging.

on bare AlO_x and AlO_x/C_{14}-PA hybrid dielectric surfaces, despite their almost identical morphology in AFM investigations (comparable domain size and step height; see SI-5), we performed XRR experiments of C_{13}-BTBT on bare AlO_x surface as well. Similar to the results on C_{14}-PA, a periodic signature of around 12 Å was observed, indicating a comparable packing in the second and third layers, with a slightly decreased order (Figure 2d). In fact, the first C_{13}-BTBT monolayer, directly on top of the AlO_x surface, presents a more disordered distribution of molecules (broad first plateau, Figure 2d). This disorder might be the reason for the relatively unfavorable transport and the reduced mobility of 2.2 $cm^2/(V{\cdot}s)$.

Additionally, we have tested the long-term stability of our devices. All devices have good shelf life stability in ambient air. More importantly, the stability during device operation (bias stress) in ambient air is very promising. We operated a device with AlO_x/C_{10}-PA dielectrics (L = 200 μm, W = 500 μm) continuously for 13 h (720 measurements). The initial mobility value (5.2 $cm^2/(V{\cdot}s)$) decreased to only 1.5 $cm^2/(V{\cdot}s)$ without a significant shift in V_{TH} and without increasing gate voltage (I_G) (SI-3).

In summary, we synthesized an asymmetric substituted 2-tridecyl[1]benzothieno[3,2-*b*][1]benzothiophene. The material behaves as an excellent p-type organic semiconductor with large hole mobilities up to 17.2 $cm^2/(V{\cdot}s)$ and promising air stability during operation. As a result of XRR investigations, we address the performance on *n*-alkyl SAM surfaces, in particular to a dense packaging of the BTBT π-system layers with periodic distances of only 13 Å close to the dielectric interface.

■ ASSOCIATED CONTENT

Ⓢ Supporting Information

Device fabrication steps; representative device output and transfer characteristics; bias stress stability measurement; and XRR, NMR, and DSC of C_{13}-BTBT. This material is available free of charge via the Internet at http://pubs.acs.org.

■ AUTHOR INFORMATION

Corresponding Author

marcus.halik@ww.uni-erlangen.de

Notes

The authors declare no competing financial interest.

■ ACKNOWLEDGMENTS

The authors gratefully acknowledge the Cluster of Excellence "Engineering of Advanced Materials" (www.eam.uni-erlangen.de) and the staff of ID10B (ESRF), especially Alexei Vorobiev, for technical assistance. This work was supported by German Research Council (DFG), DFG HA 2952/4-1, EXC 315.

■ REFERENCES

(1) Park, S. K.; Jackson, T. N.; Anthony, J. E.; Mourey, D. A. *Appl. Phys. Lett.* **2007**, *91*, 063514.
(2) Zschieschang, U.; Yamamoto, T.; Takimiya, K.; Kuwabata, H.; Ikeda, M.; Sekitani, T.; Someya, T.; Klauk, H. *Adv. Mater.* **2011**, *23*, 654.
(3) Yan, H.; Chen, Z.; Zheng, Y.; Newman, C.; Quinn, J. R.; Dotz, F.; Kastler, M.; Facchetti, A. *Nature* **2009**, *457*, 679.
(4) Minemawari, H.; Yamada, T.; Matsui, H.; Tsutsumi, J. y.; Haas, S.; Chiba, R.; Kumai, R.; Hasegawa, T. *Nature* **2011**, *475*, 364.
(5) Ebata, H.; Izawa, T.; Miyazaki, E.; Takimiya, K.; Ikeda, M.; Kuwabata, H.; Yui, T. *J. Am. Chem. Soc.* **2007**, *129*, 15732.
(6) Soeda, J.; Hirose, Y.; Yamagishi, M.; Nakao, A.; Uemura, T.; Nakayama, K.; Uno, M.; Nakazawa, Y.; Takimiya, K.; Takeya, J. *Adv. Mater.* **2011**, *23*, 3309.
(7) Halik, M.; Klauk, H.; Zschieschang, U.; Schmid, G.; Ponomarenko, S.; Kirchmeyer, S.; Weber, W. *Adv. Mater.* **2003**, *15*, 917.
(8) Shinamura, S.; Miyazaki, E.; Takimiya, K. *J. Org. Chem.* **2010**, *75*, 1228.
(9) Kosta, B.; Kozmik, V.; Svoboda, J. *Coll. Czech. Chem. Commun.* **2002**, *67*, 645.
(10) Heiszman, J.; Bitter, I.; Harsany, K.; Toke, L *Synthesis* **1987**, *8*, 738.
(11) Salinas, M.; Jäger, C. M.; Amin, A. Y.; Dral, P. O.; Meyer-Friedrichsen, T.; Hirsch, A.; Clark, T.; Halik, M. *J. Am. Chem. Soc.* **2012**, *134*, 12648.
(12) Halik, M.; Klauk, H.; Zschieschang, U.; Schmid, G.; Dehm, C.; Schutz, M.; Maisch, S.; Effenberger, F.; Brunnbauer, M.; Stellacci, F. *Nature* **2004**, *431*, 963.
(13) Amin, A. Y.; Reuter, K.; Meyer-Friedrichsen, T.; Halik, M. *Langmuir* **2011**, *27*, 15340.
(14) Smilgies, D.-M.; Boudet, N.; Struth, B.; Konovalov, O. *J. Synchrotron Radiat.* **2005**, *12*, 329.
(15) Mottaghi, M.; Horowitz, G. *Org. Electron.* **2006**, *7*, 528.
(16) Parratt, L. G. *Phys. Rev.* **1954**, *95*, 359.